

Measurement of Coherent Polarons in the Strongly Coupled Antiferromagnetically Ordered Iron-Chalcogenide $\text{Fe}_{1.02}\text{Te}$ using Angle-Resolved Photoemission Spectroscopy

Z. K. Liu,^{1,2} R.-H. He,³ D. H. Lu,⁴ M. Yi,^{1,2} Y. L. Chen,^{5,1,6} M. Hashimoto,⁴ R. G. Moore,¹ S.-K. Mo,⁶ E. A. Nowadnick,^{1,2} J. Hu,⁷ T. J. Liu,⁷ Z. Q. Mao,⁷ T. P. Devereaux,¹ Z. Hussain,⁶ and Z.-X. Shen^{1,2}

¹Stanford Institute for Materials and Energy Sciences,

SLAC National Accelerator Laboratory, Menlo Park, California 94025, USA

²Geballe Laboratory for Advanced Materials, Departments of Physics and Applied Physics, Stanford University, Stanford, California 94305, USA

³Department of Physics, Boston College, Chestnut Hill, Massachusetts 02467, USA

⁴Stanford Synchrotron Radiation Lightsource, SLAC National Accelerator Laboratory, Menlo Park, California 94025, USA

⁵Department of Physics, University of Oxford, UK

⁶Advanced Light Source, Lawrence Berkeley National Laboratory, Berkeley, California 94720, USA

⁷Department of Physics and Engineering Physics, Tulane University, New Orleans, Louisiana 70118, USA

(Dated: November 1, 2018)

The nature of metallicity and the level of electronic correlations in the antiferromagnetically ordered parent compounds are two important open issues for the iron-based superconductivity. We perform a temperature-dependent angle-resolved photoemission spectroscopy study of $\text{Fe}_{1.02}\text{Te}$, the parent compound for iron chalcogenide superconductors. Deep in the antiferromagnetic state, the spectra exhibit a “peak-dip-hump” line shape associated with two clearly separate branches of dispersion, characteristics of polarons seen in manganites and lightly-doped cuprates. As temperature increases towards the Neel temperature (T_N), we observe a decreasing renormalization of the peak dispersion and a counterintuitive sharpening of the hump linewidth, suggestive of an intimate connection between the weakening electron-phonon (e-ph) coupling and antiferromagnetism. Our finding points to the highly-correlated nature of $\text{Fe}_{1.02}\text{Te}$ ground state featured by strong interactions among the charge, spin and lattice and a good metallicity plausibly contributed by the coherent polaron motion.

PACS numbers: 74.25.Jb, 74.70.Xa, 79.60.-i, 71.38.-k

The role of many-body interactions is one of the central questions for unconventional superconductivity. For the recently discovered iron-based superconductors, the strength of electronic correlations is still an unsettled issue [1, 2]. For one of them, iron chalcogenides, a strong correlation scenario has been proposed by theory [3, 4] and supported by experiments [5–12]. For their parent compound Fe_{1+y}Te , while the high-temperature paramagnetic (PM) state shows similar signs for localized physics as in the undoped high- T_c cuprates in transport [11] and optical [12] experiments, the metallic behavior in the low-temperature antiferromagnetic (AFM) state (at $T < T_N$, $T_N = 72$ K for $y = 0.02$) [11, 13] seems, *prima facie*, to deviate from localized physics and questions the importance of strong correlations.

In terms of the strength of coupling between itinerant electrons and other degrees of freedom including the localized spins, a recent theoretical work [14] has pointed out similarities between iron chalcogenides and colossal magnetoresistive (CMR) manganites, a strongly-correlated prototype system also with a (ferro)magnetically ordered metallic ground state. A salient manifestation of strong coupling with collective modes in CMR manganites is the self-energy effect seen in the single-particle spectral function measured by angle-resolved photoemission spectroscopy (ARPES), which is

characterized by a characteristic “peak-dip-hump” line shape that has been attributed to polaron formation [15, 16]. In this letter, we present temperature-dependent ARPES study on $\text{Fe}_{1.02}\text{Te}$. Our result shows that the spectra in the AFM state contain signature of polarons reminiscent of those found in CMR manganites [15, 17] and deeply underdoped cuprates [18, 19]. This observation thus raises an intriguing perspective that the good metallicity of $\text{Fe}_{1.02}\text{Te}$ at low temperature arises from coherent polaron motion, as proposed for the manganites case [16]. Different from the manganites case, however, the temperature evolution of the polaron feature shows signs of concomitant weakening of the strong-coupling polaron behavior and the magnetic ordering upon the increase of temperature. This in turn suggests the electronic correlations likely strengthen, rather than weaken as generally thought, in the AFM state. The observed intimate tracking of polaron behavior with the magnetic ordering points to a cooperation between lattice and magnetism as a key factor driving the low-temperature system towards the strong-coupling limit.

High quality $\text{Fe}_{1.02}\text{Te}$ single crystals were synthesized using flux method [13]. Excess Fe ratio was kept as low as possible and was determined by energy-dispersive X-ray spectrometry to be around 2%. ARPES measurements were performed at beamline 5-4 at Stanford Synchrotron

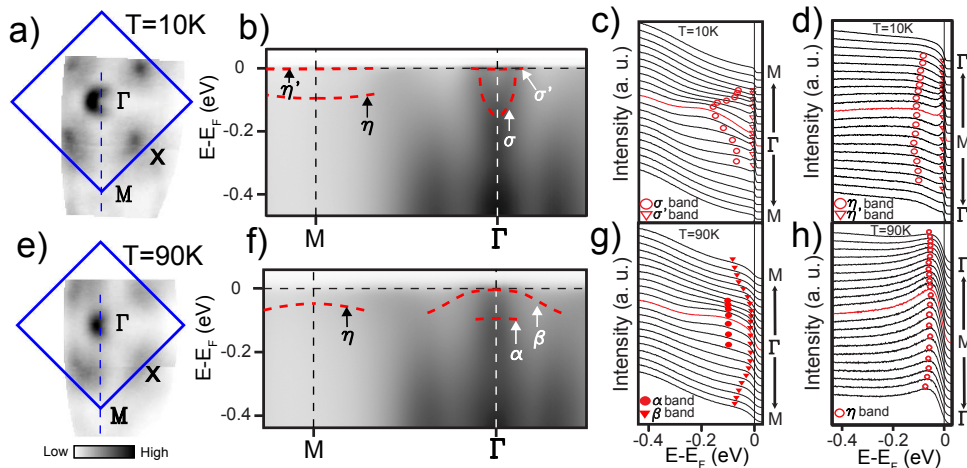


FIG. 1. (a),(e) Fermi surface map of $\text{Fe}_{1.02}\text{Te}$ measured with 22 eV excitation energy at (a) $T=10$ K and (e) $T=90$ K. The photoemission intensity is integrated over 10 meV window around the E_F . (b),(f) Photoemission intensity of the cut along the Γ -M direction of (a) and (e), respectively. Dashed curves are eyeguides of dispersion. (c),(g) Plot of the energy distribution curves (EDCs) around Γ along the cuts in (b) and (f). Labeling marks are local maxima of the EDCs after dividing the corresponding Fermi-Dirac function and background subtraction (see below). (d),(h) Plot of the EDCs around M along the cuts in (b) and (f). Labeling marks are local maxima of the EDCs.

Radiation Lightsource (photon energy $h\nu = 22$ eV). The energy(angle) resolution is 7 meV(0.3°). The samples were cleaved *in situ*, and measured in ultrahigh vacuum with pressure better than 3.0×10^{-11} Torr.

We first compare the electronic structure of $\text{Fe}_{1.02}\text{Te}$ above (90 K) and below (10 K) the AFM transition (Fig. 1). The electronic structure in the PM state [Fig. 1(e)-(h)] is characterized by overall broad features. Along the high symmetry Γ -M direction in 2-Fe unit cell Brillouin zone, we can identify two hole-like bands (α , β) around Γ and one hole-like band (η) around M. The observed band dispersions show partial agreement with the DFT calculation [20]: the β and η bands roughly follow the calculated dispersion, with the calculated bandwidth renormalized by a factor of 5. The predicted outermost hole-like band at Γ and electron-like band at M may be suppressed by the polarization matrix elements. The photoemission intensity observed around X as shown on the Fermi surface plot [Fig. 1(e)] is not predicted by the calculation. We note that we do not see well-defined hole-like band duplicating Γ feature at X as previously reported in Ref. [21]. Our spectra would be similar to those in Ref. [7] if their Brillouin zone definition is rotated by 45° [22].

Comparing with the PM state, electronic structure of $\text{Fe}_{1.02}\text{Te}$ in the AFM state is drastically different [Fig. 1(a)-(d)]: One electron-like feature is identified around the Γ point (σ band). The η band at M shifts further away from E_F . The σ and η bands are characterized by very broad humps in EDCs and do not appear to cross E_F . In the vicinity of E_F , sharp quasiparticle peaks with small spectral weight are observed at both Γ (σ' band) and M (η' band). Note that these two sharp quasiparticle

bands are not predicted in the bandstructure calculation for the AFM state [23], nor do they look like extrinsic effects (such as impurity induced features) since they only appear close to E_F where σ and η features are observed.

We next focus on the σ and σ' bands inspired by their intimate dispersion relationship observed [Fig. 2(a)-(c)]. To track the features close to and above E_F , we divide each EDC by the corresponding Fermi-Dirac function at the measurement temperature convolved with the instrument resolution [Fig. 2(a)]. We then perform background subtraction to highlight the σ and σ' features. An EDC far away from Γ where σ and σ' bands both have vanishing intensity is chosen as the background and subtracted from all the EDCs around Γ [24].

The EDC plot of the σ and σ' bands [Fig. 2(b)] show canonical two-pole spectral functions, commonly referred to as the peak-dip-hump line shape [19]. Local minima (the dips) are observed at 18 meV below E_F and break the dispersion into two branches. The high energy branch, the σ band, shows a broad hump feature which can be well fitted by a Gaussian function. The maxima of the hump overall follow the band dispersion determined by a parabolic fitting of the momentum distribution curve (MDC) peaks [Fig. 2(c)]. But it starts to deviate from the MDC derived dispersion, levels off and tends to bend back when getting close to around 60 meV below E_F . The low energy branch, electron-like σ' band, is characterized by a sharp quasiparticle peak and could be well fitted by a Lorentzian function. It also has small bandwidth: A parabolic fitting shows its effective mass of $\sim 18 m_e$ at 30 K, which is ~ 90 times larger than the band mass derived from the MDC dispersion, which was previously demonstrated to produce a band disper-

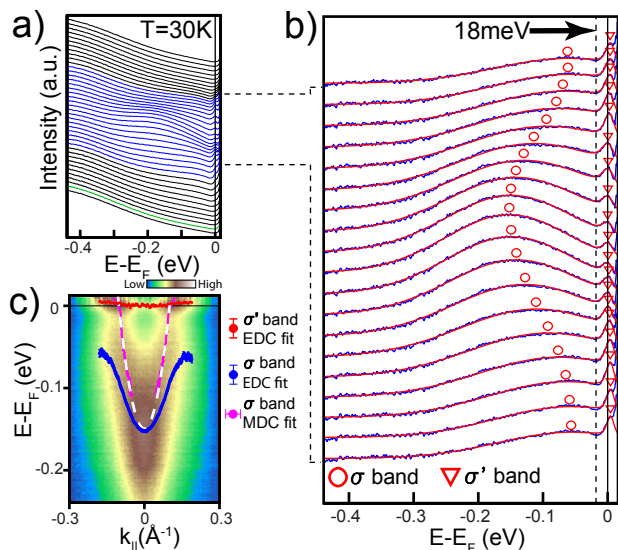


FIG. 2. (a) Plot of the EDCs around Γ along the Γ -M direction cut measured at 30 K. The data is plotted after normalizing to the intensity at the highest binding energy and dividing the corresponding Fermi-Dirac function. The green EDC is taken as the background to be subtracted from the blue EDCs around Γ . (b) Plot of the blue EDCs around Γ after background subtraction in (a). Red lines are Gaussian+Lorentzian fitting results of the EDCs. Fitted Gaussian(Lorentzian) peaks are marked by open circles(triangles). The dashed line denotes the position of the dips in the EDCs, which is 18 meV below E_F . (c) Photoemission intensity plot of the EDCs in (b), together with marks labeling the peak positions in the EDCs and MDCs. Peak positions of the MDCs of the σ band are determined by fitting to a two-Lorentzian function. The dashed curve is the parabolic fit of the σ band MDC peaks.

sion akin to the LDA predicted bareband [15]. Similar features are also observed in the η and η' bands at the M point (see below).

Such self-energy effect in the single-particle spectral function of $\text{Fe}_{1.02}\text{Te}$ bears strong resemblance to that seen in deeply underdoped cuprates [18, 19] and CMR manganites $\text{La}_{2-2x}\text{Sr}_{1+2x}\text{Mn}_2\text{O}_7$ [15, 17]. A widely-accepted interpretation for those features in cuprates and manganites is due to the strong coupling between electrons and some bosonic collective modes, which leads to the formation of, *e.g.*, polarons in the case of manganites. In this scenario, the hump feature describes the incoherent excitations of electrons strongly coupled to a bath of bosons (phonons) and the small quasiparticle peak which forms a heavily renormalized band associated with the coherent polaron motion [16]. Our observation of the peak-dip-hump structure in the spectra and large effective mass enhancement of the quasiparticle band in $\text{Fe}_{1.02}\text{Te}$ is consistent with the polaron interpretation. In such a picture, the energy scale of the involved collective mode can be estimated from the dip position in the

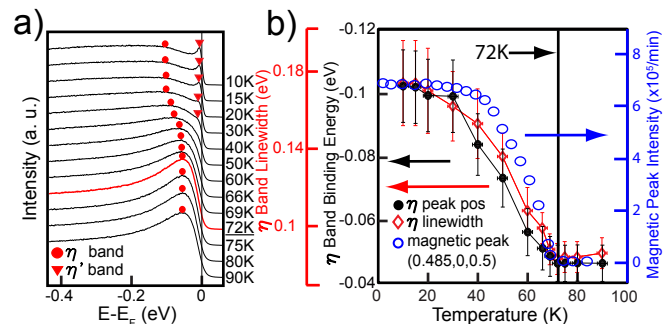


FIG. 3. (a) Plot of the EDCs at the M point at various temperatures. The red EDC is recorded when $T=T_N$. Marks labeling peaks of the η and η' bands are local maxima of the EDCs. (b) Plot of the η band binding energy and linewidth at the M point together with the (0.5, 0, 0.5) AFM Bragg peak intensity versus temperature. The magnetic peak intensity curve is adapted from a published neutron scattering experiment [29] and roughly proportional to the ordered magnetic moment of Fe.

EDCs to be about 18 meV, which is very close in energy to the A_{1g} phonon mode observed in Raman spectroscopy [25, 26] but rather different from the reported $(\pi, 0)$ magnetic resonance mode at ~ 7 meV [27, 28]. This comparison suggests that the phonon is more likely the direct agent involved in the polaron formation, but as we will see below that the e-ph coupling alone might not be sufficient.

The temperature evolution of the ARPES spectra, especially across the AFM to PM phase transition, provides deeper insights into the polaron scenario in $\text{Fe}_{1.02}\text{Te}$. In Fig. 3(a), we show the M point EDCs at various temperatures. As temperature increases, we observe distinct evolution behavior of the hump (η band) and the peak (η' band) features: the quasiparticle peak in the η' band quickly loses spectral weight and becomes indiscernible eventually for $T > 50$ K; Meanwhile, the peak in the η band first stays almost unchanged below 30 K. At $30 \text{ K} < T < T_N$, the maximum position shifts towards lower binding energy (BE) and the linewidth of the hump becomes narrower. Finally above T_N , the η band stays basically unchanged again.

The distinct behavior of the η and η' bands together reveals how polarons evolve with temperature. A similar spectral weight reduction of the quasiparticle peak is also observed in the temperature evolution of the polaron line shape in manganites [16, 30] and was interpreted therein as loss of coherence of condensed polarons. The motion of coherent polarons at low temperature has been proposed to be an important factor (in addition to the double exchange mechanism) that contributes to the low-temperature metallicity of manganites. The observed temperature dependence of the η' band is consistent with the polaron scenario and, by analogy, we propose that the coherent polaron motion might also play

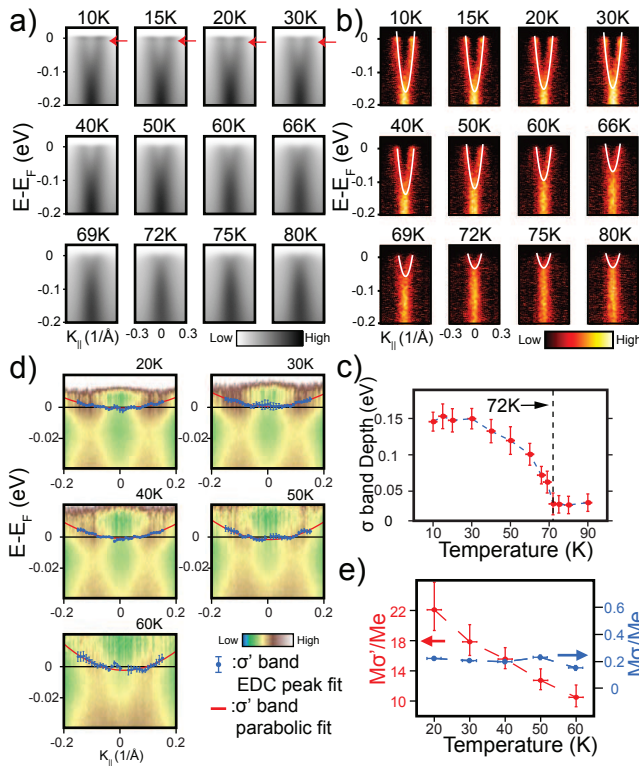


FIG. 4. (a) Photoemission intensity around Γ along the Γ -M direction at various temperatures. Red arrows indicate the positions of the dips in the spectra. (b) The second derivative plot of each intensity plot in (a). White curves are the parabolic fit of the MDC peaks found in (a). (c) Plot of the σ band depth (derived from the fitting results in (b)) versus temperature. (d) Magnified plot of photoemission intensity in the E_F vicinity at various temperatures. The data are processed using the similar method as in Fig. 2. Blue marks denote the peaks of the EDCs of the σ' band and the red curve is the parabolic fit of these peaks. (e) Plot of the effective mass of the σ' and σ band versus temperature. The effective mass of the σ' and σ band is calculated from the EDC and MDC [Fig. 4(b)] fitting results, respectively. If not shown, the error bars are smaller than the symbol's size.

an important role in the metallic transport in the AFM state of $\text{Fe}_{1.02}\text{Te}$ - an important possibility that, to our knowledge, has been overlooked so far.

The evolution of the hump (η band) feature shows some onset behaviors at the magnetic ordering transition, different from the manganite case. In manganites the humps are broader and shift to higher BE at higher temperatures [16, 30]. In contrast, in $\text{Fe}_{1.02}\text{Te}$, the humps get narrower at higher temperatures [Fig. 3(a)] - a trend opposite to the expectation for the mere thermal smearing [31] - and shift toward low BE as temperature increases. We plot the BE and the hump linewidth of the η band together with the Fe magnetic moment as a function of temperature in Fig. 3(b) and find that all of them show concomitant changes tied to T_N . The linewidth change of the hump shows the weakening of electron incoherence

(likely by phonon scattering) as Fe magnetism decreases rapidly across T_N . While the observed band shift is certainly related to the AFM ordering, it cannot be directly explained by the resulting band reconstruction, because the ordering vector is in Γ -X direction instead of Γ -M and the bandstructure calculation did not reproduce the observed shift [23]. Alternatively, this apparent band shift could be taken as a natural consequence of the disappearing of the EDC “dip” that sets the peak and hump apart at low temperatures but can no longer be clearly resolved at $T > 50$ K. Therefore, the entire evolution of the η band hump likely suggests the dissociation, rather than decoherence, of polarons, as a result of a weakened e-ph coupling upon approaching the magnetic ordering transition, which does not seem to occur in manganites.

Such a unique aspect of the polaron formation in $\text{Fe}_{1.02}\text{Te}$ is further supported by a similar temperature evolution of the σ and σ' bands observed at the Γ point, despite the complications introduced by the band reconstruction due to the AFM ordering (Fig. 4; see the supplemental material for a detailed discussion): the σ band shifts up from $\sim 150\text{meV}$ to $\sim 30\text{meV}$ below E_F and becomes a part of the β band around Γ as the temperature increases, while the “vertical dispersion” sitting at the Γ point [Fig. 4(a)&(b)] becomes more prominent at high temperatures and is identified to be the α band. The existence of the σ' band is indicated by the red arrows in Fig. 4(a) pointing to positions where the ARPES spectra break up into two dominant parts (the dips). Up to 30K the dips are clearly discernible and the positions unchanged, whereas they become increasingly obscure upon raising temperature. At $T > 60$ K (at Γ), both branches merge into one. Additionally, we could extract the effective mass of the σ' band from detailed EDC analysis at temperatures where the σ' band is discernable [Fig. 4(d)]. While the effective mass of the σ band does not show significant variation, the effective mass of the σ' band decreases as the temperature increases [Fig. 4(e)]. Such observation at Γ provides a complementary angle to see how the e-ph coupling decreases when the AFM order diminishes.

Taken collectively, the observed temperature evolutions of the polaron features at both Γ and M suggest that the e-ph coupling weakens along with the demise of the AFM. Consistent with these, a recent Raman experiment shows that the linewidth of the characteristic A_{1g} phonon mode of the appropriate energy of the dip (~ 20 meV) is broader at low temperature and narrower at high temperature, and the change is most dramatic across T_N [32].

From a theoretical perspective, antiferromagnetism could either reduce or increase the critical e-ph interaction for a polaron crossover. On one hand, carriers are slowed down due to surrounding spin flip clouds which make them subject to stronger e-ph interactions and a polaron formation at a smaller critical coupling; how-

ever, strong electronic correlations needed for antiferromagnetism can suppress charge fluctuations and the associated e-ph interaction, which would make polaron formation more difficult. This problem has been studied with several approaches in the context of the underdoped cuprates. Diagrammatic quantum Monte Carlo studies of a single hole in the t-J model coupled to optical phonons found that antiferromagnetism reduced the critical e-ph coupling for polaron formation [33]. In contrast, dynamical mean field theory studies of polaron formation in the Hubbard-Holstein model have found an increase in the critical e-ph coupling for polaron formation in both PM [34] and AFM [35] state, yet the increase is much smaller in AFM state. A study utilizing the dynamic cluster approximation has found a synergistic interplay between antiferromagnetism and polaron formation, and a reduction in the critical coupling for polaron formation [36]. These theoretical proposals suggest that the presence of antiferromagnetism helps polaron formation, compatible with our observations. Such a picture of the polaron formation as the result of a cooperative interplay among the magnetism and e-ph coupling sets $\text{Fe}_{1.02}\text{Te}$ uniquely apart from manganites.

We thank A. S. Mishchenko, A. F. Kemper, B. Moritz, D. J. Singh and J. S. Wen for enlightening discussions. This work is supported by the Department of Energy, Office of Basic Energy Sciences, Division of Materials Science. The work at Tulane is supported by the NSF under Grant No. DMR-0645305 and the LA-SiGMA program under Award No. EPS-1003897.

[1] J. Paglione and R. L. Greene, *Nat Phys*, **6**, 645 (2010).
 [2] F. Wang *et al.*, *Science*, **332**, 200 (2011).
 [3] A. M. Turner, F. Wang, and A. Vishwanath, *Phys. Rev. B*, **80**, 224504 (2009).
 [4] M. Aichhorn, S. Biermann, T. Miyake, A. Georges, and M. Imada, *Phys. Rev. B*, **82**, 064504 (2010).
 [5] A. Tamai *et al.*, *Phys. Rev. Lett.*, **104**, 097002 (2010).

[6] K. Nakayama *et al.*, *Phys. Rev. Lett.*, **105**, 197001 (2010).
 [7] Y. Zhang *et al.*, *Phys. Rev. B*, **82**, 165113 (2010).
 [8] C. C. Homes *et al.*, *Phys. Rev. B*, **81**, 180508 (2010).
 [9] A. Yamasaki *et al.*, *Phys. Rev. B*, **82**, 184511 (2010).
 [10] J. Hu *et al.*, *Phys. Rev. B*, **83**, 134521 (2011).
 [11] T. J. Liu *et al.*, *Nat Mater*, **9**, 718 (2010).
 [12] G. F. Chen *et al.*, *Phys. Rev. B*, **79**, 140509 (2009).
 [13] T. J. Liu *et al.*, *Phys. Rev. B*, **80**, 174509 (2009).
 [14] W.-G. Yin, C.-C. Lee, and W. Ku, *Phys. Rev. Lett.*, **105**, 107004 (2010).
 [15] N. Mannella *et al.*, *Nature*, **438**, 474 (2005).
 [16] N. Mannella *et al.*, *Phys. Rev. B*, **76**, 233102 (2007).
 [17] Z. Sun *et al.*, *Phys. Rev. Lett.*, **97**, 056401 (2006).
 [18] K. M. Shen *et al.*, *Phys. Rev. Lett.*, **93**, 267002 (2004).
 [19] A. Damascelli *et al.*, *Rev. Mod. Phys.*, **75**, 473 (2003).
 [20] A. Subedi, L. Zhang, D. J. Singh, and M. H. Du, *Phys. Rev. B*, **78**, 134514 (2008).
 [21] Y. Xia *et al.*, *Phys. Rev. Lett.*, **103**, 037002 (2009).
 [22] We used X-ray diffraction to align the samples, in such a way that is justified by a comprehensive Se-concentration dependence study of the band structure of $\text{Fe}_{1+y}\text{Se}_x\text{Te}_{1-x}$, which will be reported elsewhere.
 [23] F. Ma, W. Ji, J. Hu, Z.-Y. Lu, and T. Xiang, *Phys. Rev. Lett.*, **102**, 177003 (2009).
 [24] A. Kaminski *et al.*, *Phys. Rev. B*, **69**, 212509 (2004).
 [25] T.-L. Xia *et al.*, *Phys. Rev. B*, **79**, 140510 (2009).
 [26] K. Okazaki, S. Sugai, S. Niitaka, and H. Takagi, *Phys. Rev. B*, **83**, 035103 (2011).
 [27] I. A. Zaliznyak *et al.*, *Phys. Rev. Lett.*, **107**, 216403 (2011).
 [28] C. Stock, E. E. Rodriguez, M. A. Green, P. Zavalij, and J. A. Rodriguez-Rivera, *Phys. Rev. B*, **84**, 045124 (2011).
 [29] O. J. Lipscombe *et al.*, *Phys. Rev. Lett.*, **106**, 057004 (2011).
 [30] S. de Jong *et al.*, *Phys. Rev. B*, **76**, 235117 (2007).
 [31] M. Hashimoto *et al.*, *Nat Phys*, **6**, 414 (2010).
 [32] V. Gnezdilov *et al.*, *Phys. Rev. B*, **83**, 245127 (2011).
 [33] A. S. Mishchenko and N. Nagaosa, *Phys. Rev. Lett.*, **93**, 036402 (2004).
 [34] G. Sangiovanni, M. Capone, C. Castellani, and M. Grilli, *Phys. Rev. Lett.*, **94**, 026401 (2005).
 [35] G. Sangiovanni, O. Gunnarsson, E. Koch, C. Castellani, and M. Capone, *Phys. Rev. Lett.*, **97**, 046404 (2006).
 [36] A. Macridin, B. Moritz, M. Jarrell, and T. Maier, *Phys. Rev. Lett.*, **97**, 056402 (2006).